Wide area fuzzy controller with latency compensation in order damping of sub synchronous resonance in DFIG based wind farms

YASER BOSTANI[1,*] **AND SAEID JALILZADEH**[1]

[1] *Department of Electrical Engineering, University of Zanjan, Zanjan, Iran*
[*] *Corresponding author: y.bostani@gilrec.co.ir*

Manuscript received 04 September, 2021; revised 11 November, 2021; accepted 16 December, 2021. Paper no. JEMT-2109-1331.

This paper offers a new auxiliary damping control approach based on the wide area measurement system (WAMS) totally to depress sub-synchronous resonance (SSR) in doubly-fed induction generator (DFIG), which is primarily based on wind farms linked to series capacitive compensated transmission networks. In addition, wide area measurement systems have caused their use in power systems with the advancement of technology. However, the delay in sending measurement signals is considered as an important point in spite of all of its benefits if this latency could go to pot the damping overall performance of control approach. This paper presents a fuzzy approach damping controller (FLWADC) to mitigate SSR for the time delay. The FLWADC is a supplementary signal at the stator voltage of the gird-side converter (GSC) of DFIG- based wind farms FLWADC executed by using voltage and the present day of compensating series capacitive because of its established robustness against input sign versions inside the proposed manipulated approach. The effectiveness and validity of the proposed additional damping control were verified on a modified version of the IEEE first benchmark model via time simulation analysis by using Matlab/Simulink.

keywords: *Doubly fed induction generator, fuzzy controller, wade area measurement systems, latency, sub synchronous resonance.*

http://dx.doi.org/10.22109/jemt.2021.303212.1331

NOMENCLATURE

Wb	Synchronous Speed.
$Twind$	Wind torque.
Wt	Wind turbine Speed .
Pr	Active power of the RSC converter.
Pg	Active power of the GSC converter.
Rs	Stature resistance.
Rr	Rotor resistance.
Te	Electric torque of the generator.
i_{qs}	Stator's currents in the qd0-frame.
i_{ds}	Stator's currents in the qd0-frame.
i_{qr}	Rotor's currents in the qd0-frame.
i_{dr}	Rotor's currents in the qd0-frame.
V_{qs}	Stator's voltages in the qd0-frame.
V_{ds}	Stator's voltages in the qd0-frame.
V_{qr}	Rotor's voltages in the qd0-frame.
V_{dr}	Rotor's voltages in the qd0-frame.
X_M	Magnetic reactance.
X_{lr}	Rotor leakage reactance.
X_{ls}	Stator leakage reactance.
ω_b	Synchronous frequency.
ω_r	Rotor frequency.
ω	Base frequency.
f_s	Synchronous frequency.
f_n	Natural frequency.
f_r	Rotor electrical frequency.

Abbreviations

SSR	Sub-synchronous resonance.
$wams$	Wide area measurement system.
pmu	Phasor measurement unit.
IGE	Inductive generating effects.
$DFIG$	Doubly fed induction generator.
TI	Torsional interference.
IGE	Induction generator effect.
GSC	Gird side convertor.
RSC	Rotor side convertor.

1. INTRODUCTION

Todays, an energy tool brand as new intruding renewable assets has become more complicated due to the deregulation strength and extra pressured transmission strains. Regarding the sizeable boom state-of-the-art wind farms, the most transmission in their manufacturing power is a major factor in strength structures [1]. Most of the strategies for growing the transmission energy of the strains has low cost by using capacitive series repayment [2]. The compensation stage state-of-the-art the transmission lines linked to doubly fed induction generator (DFIG)-based totally wind farms isn't excessive enough. If the DFIG-based totally wind farm becomes in series with the capacitive series compensated transmission line, the possibility latest the sub synchronous resonance (SSR) phenomenon occurring will growth state-of-the-art the excessive inductive houses present day DFIGs [3]. SSR phenomenon is divided into induction generator effect (IGE) and torsional interplay (TI) in wind farms interfaced with series compensated community. In reality, induction generator effect (IGE) of the network resonant oscillatory mode is the predominant motive SSR of the present day [2]. Low shaft stiffness present day wind turbine pressure educate ends in low frequency torsional modes [9], which hardly ever have interaction with the community resonant modes in the electric machine. in wind generators, the frequency contemporary torsional modes can be as little as 1-3 Hz. with the intention to have torsional interplay, the community mode must have a frequency contemporary fifty-seven- fifty-nine Hz [3]. Accordingly, this calls for a completely excessive level present day series compensation which hardly ever occurs.

So far, a large number of studies have been conducted in the field of SSR [4–19]. Some focused on damped oscillation of SSR using an additional controller in RSC, GSC, and DFIG based wind farm converters, while some emphasized damped SSR using a FACTS device replaced with a series capacitor and applied control to these devices. However, WAMS is widely used in power systems during the recent years. For instance, In [20], The use of WAMS has become an indispensable practical topic in monitoring and controlling the large-scale power system. The role and the functions of PDC and PMU in WAMS were summarized. A WADC-PSS was designed based on modal analysis and using PSO method. WADC-PSS input signals are the non-local machine speed measurements from the WAMS. Also, in [21] discusses how techniques from reinforcement learning (RL) can be exploited to transition to a model-free and scalable wide-area oscillation damping control of power grids. In addition, present two control architectures with distinct features. The use of WAMS is justified since the DFIG based wind farm is usually offshore and far from the compensated power system and transmission line [23], which is important since the additional controller is for SSR attenuation in DFIG controllers, and this study used voltage and compensator capacitor voltage variations for additional controller inputs. In fact, the measurement of input quantities in WAMS is done by the using phasor measurements units (PMU), which is one of the main components of WAMS. However, the delay of measurement signals by the PMU should be considered in designing the controller. The controller may even cause instability while ignoring the latency [24].

In the above studies, extensive fuzzy controller was proposed to reduce the impact of sub-synchronous resonance for DFIG-based wind farms by considering time latencies in communication Networks. In this regard, WAFC was designed based on Mamdani inference structures in which voltage and compensator capacitor voltage variations are considered inputs for additional controller to the controller, and GSC brand new DFIG is the output.

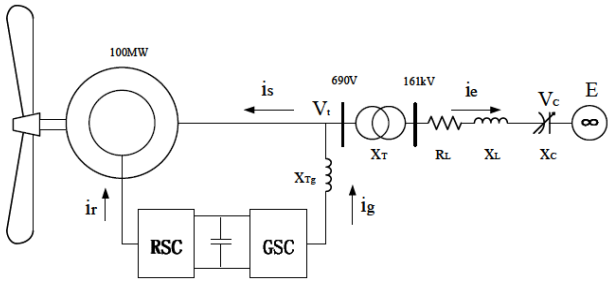

Fig. 1. Single Line Diagram of the studied system.

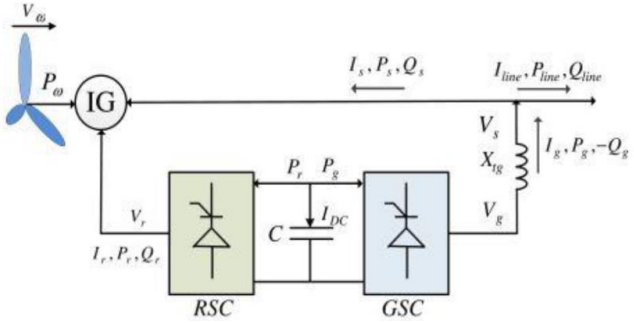

Fig. 2. Single Line model of DFIG.

The remainder of this paper is as follows. Section 2 describes the studied modeling system. Section 3 offers the background for the SSR phenomenon in fixed series compensated DFIG and the eigenvalues of the system are obtained. Section 4 describes designing wide area fuzzy logic controller (FLWADC) based on Mamdani inference system. Section 5 discusses the case study and time domain simulation end result. Finally, the conclusions are made in Section 6.

2. MODELING OF STUDIED SYSTEM

A wind power plant with DFIG is used to analyze the dynamic stability and SSR phenomenon, which is connected to an infinite bus with a compensated transmission line of capacitive series which is the modified IEEE as the first benchmark (1).

As reported in [34-37], a wind farm can be modeled as an equivalent wind farm because all of the parameters of a wind farm are similar to an equivalent wind farm. The total power is equal to the total installed capacity of wind turbines. For example, a wind farm with fifty 2 MW generators is modeled as a 100 MW generator [14].

A. Equations of induction generator in dq0 frame

Induction generator in dq0 reference frame is in the form of modeling equations (**??**) [11]:

$$X = AX + BU \tag{1}$$

$$X = \left[i_{qs} \;.\; i_{ds} \;.\; i_{qr} \;.\; i_{dr}\right]^T \tag{2}$$

$$U = \left[V_{qs} \;.\; V_{ds} \;.\; V_{qr} \;.\; V_{dr}\right]^T \tag{3}$$

$$\frac{d}{dt}\begin{bmatrix} i_{qs} \\ i_{ds} \\ i_{os} \\ i_{qr} \\ i_{dr} \\ i_{or} \end{bmatrix} = A\begin{bmatrix} i_{qs} \\ i_{ds} \\ i_{os} \\ i_{qr} \\ i_{dr} \\ i_{or} \end{bmatrix} + B\begin{bmatrix} V_{qs} \\ V_{ds} \\ V_{os} \\ V_{qr} \\ V_{dr} \\ V_{or} \end{bmatrix} \quad (4)$$

$$A = -\omega_b G^{-1} F \quad (5)$$

$$B = \omega_b G^{-1} \quad (6)$$

$$G = \begin{bmatrix} X_{ss} & 0 & 0 & X_M & 0 & 0 \\ 0 & X_{ss} & 0 & 0 & X_M & 0 \\ 0 & 0 & X_{ls} & 0 & 0 & 0 \\ X_M & 0 & 0 & X_{rr} & 0 & 0 \\ 0 & X_M & 0 & 0 & X_{rr} & 0 \\ 0 & 0 & 0 & 0 & 0 & X_{lr} \end{bmatrix} \quad (7)$$

$$F = \begin{bmatrix} R_s & \frac{\omega}{\omega_b}X_{ss} & 0 & 0 & \frac{\omega}{\omega_b}X_M \\ -\frac{\omega}{\omega_b}X_M & R_s & 0 & -\frac{\omega}{\omega_b}X_M & 0 \\ 0 & 0 & R_s & 0 & 0 \\ 0 & \frac{(\omega-\omega_r)}{\omega_b}X_M & 0 & R_r & \frac{(\omega-\omega_r)}{\omega_b}X_{rr} \\ -\frac{(\omega-\omega_r)}{\omega_b}X_{rr} & 0 & 0 & -\frac{(\omega-\omega_r)}{\omega_b}X_M & R_r \end{bmatrix} \quad (8)$$

The state space matrix of the induction generator relation can be expressed as (4), that, shows variables, which are the same as the stator and rotor currents at the two axes d and q. The items of Equation (4) defined by (5) and (6). Also, G and F of equations (5) and (6) defined by (7) and (8).

where ω_b shows synchronous frequency whose value is equal to 314 radians per second, w is the Angular Frequency of the rotating frame as dq0, R_s indicates stator resistance, and Rr is considered as the resistance of the rotor. In addition, Xm, Xls, Xlr, X_{ss} and X_{rr} indicate magnetic reactance, stator leakage reactance, rotor leakage reactance , total stator reactance, and total rotor reactance, respectively. All values are in terms of the per-unit system (pu).

B. modeling wind turbine shaft

In the SSR study, the turbine shaft model is equivalent to two masses, which reduces the volume of calculations in addition to sufficient accuracy. In this model, the low-speed mass is connected to the wind turbine shaft and the high-speed mass is connected to the generator rotor shaft [12].

$$\frac{d}{dt}\begin{bmatrix} \omega_t \\ \omega_r \\ T_{tg} \end{bmatrix} = \begin{bmatrix} \frac{(-D_t-D_{tg})}{2H_t} & \frac{D_{tg}}{2H_t} & -\frac{1}{2H_g} \\ \frac{D_{tg}}{2H_g} & \frac{(-D_t-D_{tg})}{2H_t} & \frac{1}{2H_g} \\ K_{tg}.\omega_b & -K_{tg}.\omega_b & 0 \end{bmatrix} \times \begin{bmatrix} \omega_t \\ \omega_r \\ T_{tg} \end{bmatrix} + \begin{bmatrix} \frac{T_{wind}}{2H_t} \\ \frac{T_e}{2H_g} \\ 0 \end{bmatrix} \quad (9)$$

where Wt represents the speed of wind turbine, Wr indicates the speed of the generator rotor, and Ttg stands for torsional torque or internal torque between two objects. Twind is considered as the torque generated by the wind and Te is the electric torque of the generator. All variables in relations are in unit value (Per-unit). The wind turbine electrical torque is calculated from Equation (10). The reference electrical torque is determined for obtaining the maximum PowerPoint (MPPT), as shown in Table 1. The amount of rotor speed, turbine power, and electric torque are calculated at each wind speed.

$$T_e = 0.5X_m\left(i_{qs}i_{dr} - i_{ds}i_{qr}\right) \quad (10)$$

Table 1. MPPT Lookup table.

Vw(m/s)	7	8	9	10	11	12
ω r(pu)	0.75	0.85	0.95	1.05	1.15	1.25
Pwind(pu)	0.32	0.49	0.69	0.95	1.25	1.6
Twind=Pwind/ω r	0.43	0.58	0.73	0.9	1.09	1.28

C. model of DFIG converter controllers

DFIG converters require dynamic modeling (Fig. 2). To dynamically model and study the SSR phenomenon, the controllers are used for controlling the RSC and GSC converters (Fig. 3). In addition, MPPT is applied for the RSC controller with the help of the Lookup table and is considered in the turbine shaft model for wind torque (Twinds).

D. model of DC link Capacitor DFIG converter controllers

The DC loop capacitor dynamic between DFIG converters are modeled as first-order relationships as shown in Equations (11, 12, 13). Furthermore, ir and ig are the output currents of two converters, RSC and GSC, respectively. Fig. 4 shows how power is distributed in the DC loop between RSC and GSC converters.

$$cV_{DC}\frac{dV_{DC}}{dt} = -\left(P_r + P_g\right) \quad (11)$$

$$P_r = 0.5\left(V_{qr}i_{qr} + V_{dr}i_{dr}\right) \quad (12)$$

$$P_g = 0.5\left(V_{qg}i_{qg} + V_{dg}i_{dg}\right) \quad (13)$$

where Pr shows the true power of the RSC converter, and Pg indicates the active power of the GSC. Vr and VG are the output voltages of the two converters RSC and GSC, respectively.

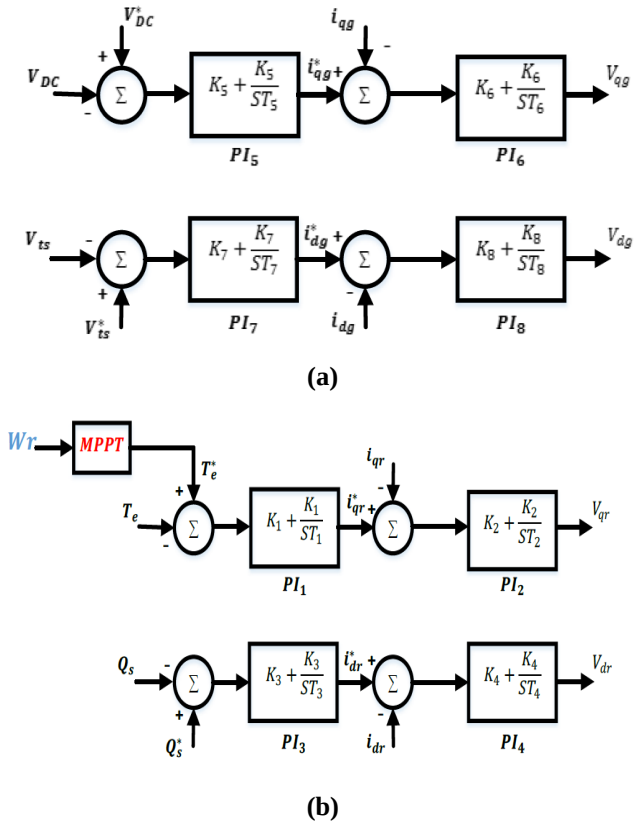

Fig. 3. GSC Controller (a) and RSC Controller (b) wind turbine with DFIG.

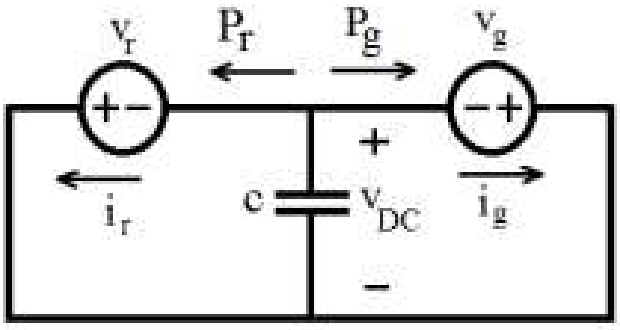

Fig. 4. DC link Capacitor of DFIG.

E. Differential equations of the capacitive series-compensated line

In this study, the transition with a grade 4 of the model of differential equations is expressed as equation 14 [12]:

$$\begin{bmatrix} \dot{I}_{qL} \\ \dot{I}_{dL} \\ \dot{V}_{qc} \\ \dot{V}_{dc} \end{bmatrix} = \begin{bmatrix} \frac{-R_L}{X_L}\omega_b & -\omega & -\frac{1}{X_L}\omega_b & 0 \\ \omega & \frac{-R_L}{X_L}\omega_b & 0 & -\frac{1}{X_L}\omega_b \\ \omega_b X_c & 0 & 0 & -\omega \\ 0 & \omega_b X_c & \omega & 0 \end{bmatrix} \begin{bmatrix} I_{qL} \\ I_{dL} \\ V_{qc} \\ V_{dc} \end{bmatrix} + \begin{bmatrix} \frac{1}{X_L}\omega_b & 0 \\ 0 & \frac{1}{X_L}\omega_b \\ 0 & 0 \\ 0 & 0 \end{bmatrix} \begin{bmatrix} V_{qs} - E_{qB} \\ V_{ds} - E_{dB} \end{bmatrix} \quad (14)$$

where V_{qc} and V_{dc} are the series capacitor voltages and currents. V_{qs} , V_{ds} , E_{qB} , and E_{dB} are the stator and infinite bus voltages. All of these parameters are shown in the qd0-frame.

3. SSR AND METHODS OF ITS ANALYSIS

Now, the consent of SSR is examined. Eigen value is explained as the method of analysis for linear system. Finally, intelligent methods are reviewed for fuzzy logic.

A. Differential equations of the capacitive series-compensated line

The SSR phenomenon is the state in which the wind plant exchanges in one or more natural frequencies with the electrical grid. This phenomenon can cause damages when it is not prevented. The SSR phenomenon is related to inductive generating and torsional interference effects. In a network with capacitive series compensation, the network has a natural frequency which is calculated by Equation (15), where f_n is the resonant frequency called sub-synchronous, and its unit is hertz. f_s shows synchronous frequency and Xl are the total reactance of the inductor, transformers, and inductor (Figure 1). Xc indicates the reactance of a series capacitor, which is a percentage of the reactance, and Xl is called the compensation percentage (% K). Due to frequency f_n, slip Sn is introduced according to Equation (16) [10, 18].

$$fn = fs\sqrt{\frac{Xc}{Xl}} \quad (15)$$

$$Sn = \frac{fn - fr}{fn} \quad (16)$$

Since S_n is usually negative, the equivalent resistance of the rotor at the sub-synchronous frequency (Req/Sn) is negative. In other words, f_r is negative when the amplitude of this resistor is more than the sum of the network and armature resistors.

As shown in Equation (17) of the second part, the current of the whole system will have an exponential function with a positive power. Sub-synchronous component with frequency (Rsys) appears in the currents and voltages of the stator and mains circuit with the existence of capacitive series compensator. The complementary frequency of this component appears as IGE in

the rotor current [15].

The torsional interference (TI) effect occurs when the frequency of the torsional mode between the two masses of the rotor shaft with a complementary frequency of the network (fs-fn) is equal or close to each other. The frequency of the torsional modes of their rotors is low due to the low stiffness of the rotor shafts of wind farms. Thus, SSR occurs in wind powe due to the effect of torsional interference (TI). Thus, there is a need for a very high level of compensation [17]. In addition, the probability of its occurrence is very low since it requires very high compensation [38].

$$i(t) = \mathrm{A}\sin(2\pi f_s \mathrm{t}) + e^{\frac{R_{eq}}{L}t} B\sin(2\pi f_n \mathrm{t} + \partial) \qquad \textbf{(17)}$$

B. Eigenvalue of System

The general state space of the network is modeled around its equilibrium point, depending on wind speed and level of compensation of the capacitor of series using the Linmod command obtained in MATLAB software. In this regard, 20 eigenvalues are obtained from the general state space of the network [17], among which four eigenvalues for induction machine, three for shaft system, eight for RSC and GSR of DfIG, four for transmission line with series capacitor, and one for dc link which form the 20th degree model. Table 2 indicates the system eigenvalues for compensation level of 70% and wind speed of 8m/s. As shown, the real values of all modes are negative except for the $\lambda 1$, $\lambda 2$ modes, which represents the sub-synchronous mode for the instability of this mode.

Table 2. Eigenvalues for compensation level 75% and wind speed 7m/s

Mode	Eigenvalues	Mode	Eigenvalues
$\lambda 1$	+0.273+j123.26	$\lambda 11$	-0.023+j30.56
$\lambda 2$	+0.273-j123.26	$\lambda 12$	-0.023-j30.56
$\lambda 3$	-6.152+j628.42	$\lambda 13$	-109.6
$\lambda 4$	-6.152-j628.42	$\lambda 14$	-568.235
$\lambda 5$	-9. 412+j95.78	$\lambda 15$	-89.65
$\lambda 6$	-9. 412-j95.78	$\lambda 16$	-0.45
$\lambda 7$	-1.150+j4.260	$\lambda 17$	-0.254
$\lambda 8$	-1.150-j4.260	$\lambda 18$	-22.02
$\lambda 9$	-189.210-j1245.45	$\lambda 19$	-14.25
$\lambda 10$	-189.210+j1245.45	$\lambda 20$	-0.003

C. Review of fuzzy system

Fuzzy logic is considered as a method for reasoning which is similar to the way humans make reason. The fuzzy logic approach mimics the human decision-making method, in which all possible intermediate states between the digital values of "yes" and "no" are considered. Fuzzy logic has four main parts, as discussed below [23].

Rule base: This section includes all of the rules and conditions which are specified as "if then" by an expert to be able to control the decisions of a "decision-making system". Based on the new methods in fuzzy theory, it is possible to adjust and reduce the rules and regulations so that the best results can be obtained with the least rules.

Fuzzifire: In the fuzzy step, the inputs are converted to fuzzy information. In other words, the numbers and information to be processed will become fuzzy sets and numbers. Input data are measured, for example, by sensors in a control system, which are modified and prepared for fuzzy logic processing.

Inference engine: In this section, the degree of compliance of fuzzy input with the basic rules is determined. In this way, different decisions are generated as a result of the fuzzy inference engine based on the percentage of compliance.

Defuzzifire: In the last step, the results of fuzzy inference, which are fuzzy sets, are converted into quantitative data. At this stage, you choose the best decision according to the outputs, which include different decisions with different percentages of compliance. This choice is normally based on the maximum degree of compliance. Fig. 5 shows all of the above-mentioned parts [24]:

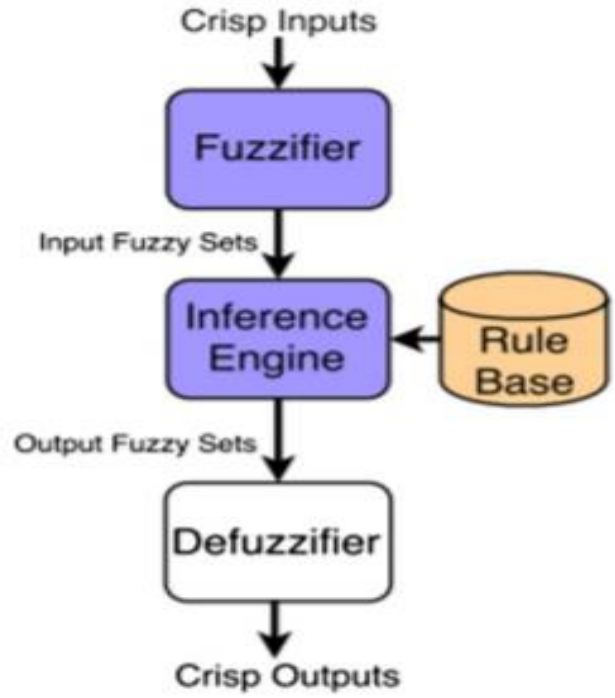

Fig. 5. Model of fuzzy system.

4. MODELLING OF WIDE AREA FUZZY CONTROLLER IN THE SYSTEM UNDER STUDY

A. Review on Wade Area Measurement Systems

By combining the capabilities of telecommunication systems and digital measuring devices and controllers, WAMS enables the monitoring, protection, and control of the smart grid over a wide area. In general, WAMS consists of three subsystems including measurement, telecommunication, and processing. The system consists of several PMUs and one or more PDCs connected by a high-speed telecommunications network, as shown in Fig. 6[23].

B. fuzzy controller based on wide area measurement system

In the hierarchical structure of the WAMS proposed in [23], the communication network is an optic fiber mesh net based on the wave-length division multiplexing (WDM) technology. As can be seen in Fig. 6, the WAMS is divided into several regional networks. Each region consists of a number of system buses and their emanated transmission lines. As it can be

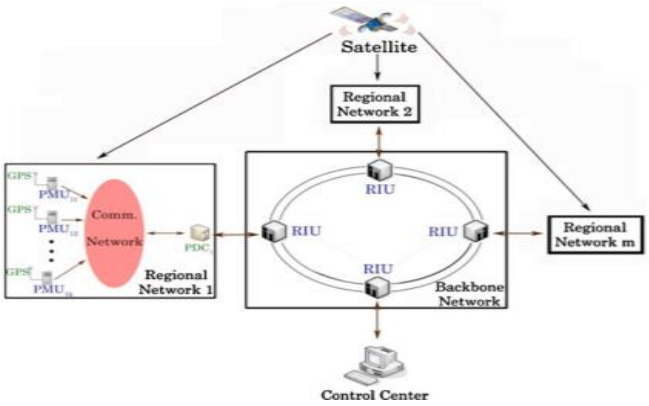

Fig. 6. Hierarchical structure of a WAMS.

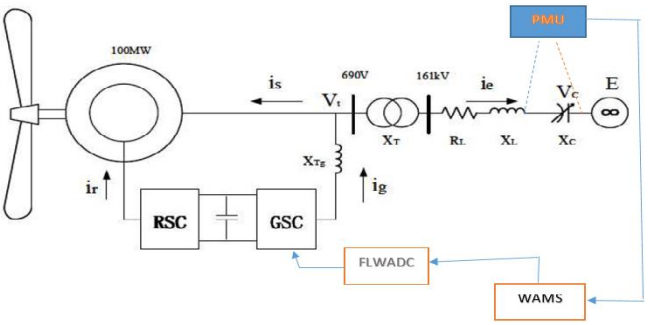

Fig. 7. Location of Fuzzy logic based on wade area in studed model.

understood from this hierarchical structure, the geographical position of the system buses is a significant factor which should be considered in the power system partitioning. Therefore, it is imperative that the system buses in a regional network be geographically close to each other. This accordingly decreases the data transmission delay and increases the reliability of the communication network. The required data by operator for various operational decisions, such as restorative actions, is another factor in the power system partitioning.

This section is to demonstrate the ability of FLC in damping SSR with using WAMS signals. The IEEE Modified first benchmark test system, shown in Fig. 1, is utilized as the study test bed and its parameters are specified in [1]. In this study, in order to attenuate the fluctuations caused by SSR, a wide area fuzzy controller called FLWADC controller has been used. This controller is applied to the output voltage control section of the stator of the terminal voltage generator (GSC converter controller).
Figure 7 shows the location of the fuzzy controller, which is applied to the input of the stator voltage control loop of GSC.
The fuzzy controller is based on the Mamdani inference model. Fuzzifier, Defuzzifier and inference methods and fuzzy rules are the main parts of the controller. The input of the fuzzy system consists of two capacitor voltage signals of the compensator and the current passing through the capacitor, which is the same as the capacitor derivative, apply. In fact, a fuzzy model of a system is designed based on complete prior knowledge of that system.

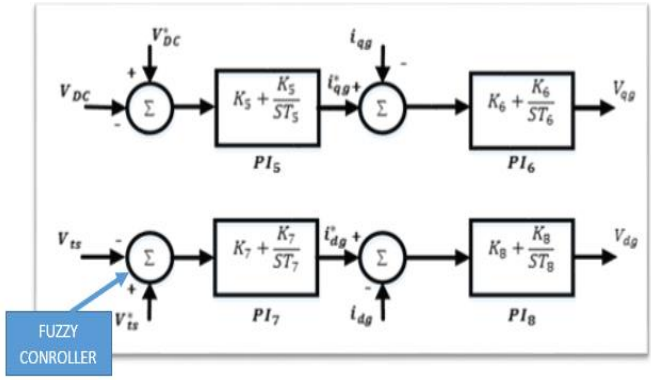

Fig. 8. Location of Fuzzy logic System.

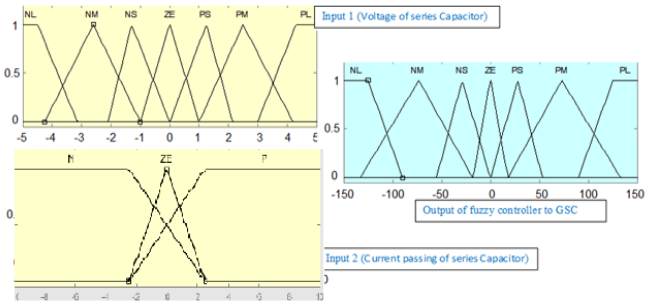

Fig. 9. Inputs and output membership functions.

The developed FLWADC is designed based on Mamdani inference engine [24]. The fuzzification process, defuzzification, rule base, and inference engine are essential parts of fuzzy controller which are clarified in the following.

B.1. fuzzification

Fuzzification involves mapping crisp input parameters, namely Vc and Ic , to fuzzy variables. This process executes a membership grade to translate the numeric values of inputs into linguistic values. Fuzzy sets for input parameters and output variables are designed by studying the behavior of FLWADC input signals in different situations. Doing so, the membership functions for inputs and output of FLC are obtained, as depicted in Figs. 9. Note that through a trial and error process with various functions, it was found that triangular membership function leads to a better damping effect for small angle deviations; thus, it is adopted for both input and output variables. In Figs. 3, the symbols are defined as Nl: negative large, NM: negative medium, NS: negative small ZE: zero, PS: positive small, PM: positive medium, PL: positive large, N: negative, ZE:zero, P: positive.

B.2. Rule Base and Inference Engine

As mentioned, the fuzzy rules are based on Mamdani type, in the form of if . . . then, and in the form of 21 fuzzy relations according to the inputs and outputs of the fuzzy system, as shown in Table 3. As shown in Table 3, if Vc is NS and dVc/dt is N, then the output is NM. Finally, the output of the fuzzy system should be converted to a crisp number. In this study, the average center of gravity was used.

Table 3. Fuzzy rules based on fuzzy system inputs and output

Vc / dVc/dt	P	N	ZE
PL	PL	PL	PL
PM	PL	PS	PM
PS	PM	ZE	PS
ZE	PM	NM	ZE
NS	ZE	NM	NS
NM	NS	NL	NM
NL	NM	NL	NL

B.3. Defuzzification

Here, it is intended to generate a crisp numeric value, which is used as a control input for power system, based on outputs of fuzzy rules. Once the input variables are fuzzified and sent to the fuzzy rule base, the output of the rule base is then aggregated and defuzzified. Aggregation means all of the output fuzzy sets are added in a logical way. Then, a crisp control signal is accordingly produced. Centroid technique, as one of the commonly used defuzzification methods, is adopted in this paper.

5. RESULTS OF TIME DOMAIN SIMULATION

IEEE first benchmark modified DFIG based wind farm system was used to evaluate the proposed controller, and MATLAB/simulink software was applied for simulating the time of the studied system. As mentioned before, the percentage of compensation of the transmission line is considered as one of the influential factors in SSR fluctuations, which increases with the percentage of compensation of the system towards instability. The modes of the studied system were expressed by using the eigenvalues method in Table 2, indicating that $\lambda 1$ and $\lambda 2$ are the oscillation modes of the system in the case where the compensation percentage is 75, as represented in Table 4.

$$\begin{aligned} &K\% \uparrow \rightarrow X_c \uparrow \rightarrow f_n = f_s\sqrt{\tfrac{X_c}{X}} \uparrow \rightarrow \\ &s_n = \tfrac{f_n - f_r}{f_n} \uparrow \rightarrow R_{eq-r} = \tfrac{R_r}{s_n} \uparrow \rightarrow R_{eq} \leq 0 \end{aligned} \quad \textbf{(18)}$$

Also, in the table 4, the sub-synchronous mode of the studied system is level 75% of compensation and wind speed 7m/s.

Table 4. SSR mode and eigenvalues for compensation level 75% and wind speed 7m/s

Resonance Frequency	SSR Mode ($\lambda 1$, $\lambda 2$ Table 1)	Level of Compensation (%)
37.56	+11.650+j130.21	75

Fig. 10 shows the compensation system in the case where the compensation percentage is 25% and the system is stable. In the third second of the simulation, the compensation percentage increases to 75 and the parameters are unstable.

A. FLWADC without latency compensation

This part of the simulation shows the application of fuzzy controller to the studied system in the case where the delays caused by the measured PMU signals are ignored. As shown in Figure 7, SSR fluctuations are damped by applying a controller to the stator voltage control loop in the GSC. The membership functions of Fig. 5 is quenched by the SSR fluctuations with the 21 fuzzy rules in Table 33 and receiving the controller inputs, which is the same as the capacitor compensating voltage and its changes from the PMU, as shown in Fig. 11.

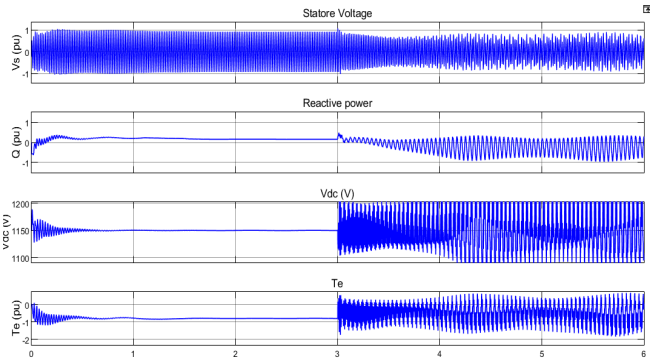

Fig. 10. capacitor voltage, reactive power stator voltage and electrical torque in k=25% to k= 75% &v=7m/s without damping.

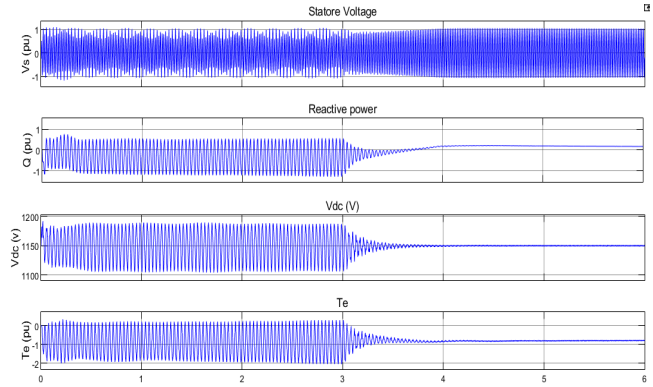

Fig. 11. Damping of capacitor voltage, reactive power and stator and electrical torque in k=75% & v=7m/s with FLWADC (ignoring time delay).

As displayed in Fig. 11, the oscillations are damped in the case where the compensation percentage is 75 and the system is unstable in the third second of the simulation by applying a fuzzy controller (FLWADC).

B. Robust FLWADC with Latency Compensation

In the previous section, WAMS-based fuzzy controller simulations were performed in which the latencies due to PMU measurement signals were ignored. In fact, these time delays in sending signals to the controller cannot be ignored since delays are inevitable in telecommunication systems [21], as shown in Table 5. Thus, these delays are ignored. As displayed in Fig. 12, it aauses system instability, which shows the state that the measurement signals applied to the fuzzy controller have a delay of 350 ms and the actions of the controller in the first second caused system instability and failed to dampen the system.

Table 5. Delay values in various communication links [23, 24]

Communication link	Associated delay (ms)
Fiber- optic cables	100-150
Digital microwave link	100-150
PLC	150-350
Telephone Lines	200-350
Satellite link	500-700

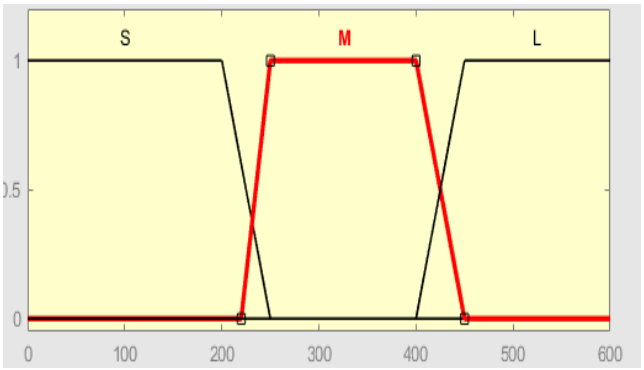

Fig. 12. Membership functions of the third input variable for robust FLWADC.

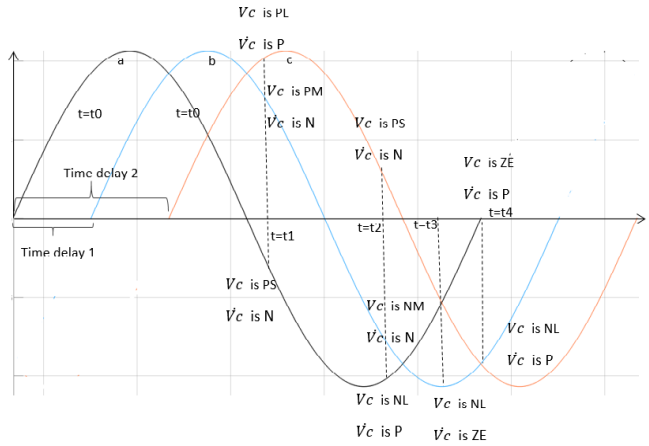

Fig. 13. Time delay signal of Vc.

To consider the delays caused by measuring PMU signals, the third input is modeled for another fuzzy input to the fuzzy controller (Figure 13). As shown, delays are considered in small (S), medium (M) and large (L) membership model. For simplicity, low delays (S) are equivalent to no delays.

The fuzzy rules of Table 3 change for applying this fuzzy input to the fuzzy system, the cause of which is shown in Fig. 14. In addition, the series compensating capacitor voltage are demonstrated in without delay (a), medium delay (b) and long delay (c) modes.

Consider the moment t = t1 as an example. At this point, the main signal is the no-delay input of Vc is Ps and $(Vc)\cdot$ is N, which means that the output value of the fuzzy controller equals to ZE. However, if the medium delay is (M: Time delay 1), the fuzzy rule in this delay is Vc is PM and $(Vc)\cdot$ is N, which should be the output of system the ZE. Further, if the delays are large, L is time delay 2, and the fuzzy rule in this delay is Vc is PL and $(Vc)\cdot$ is P, which should be the output of the fuzzy system in this delay, which is ZE. Similarly, other modified fuzzy rules are shown by considering the delays in Table 6.

By changing the fuzzy rules which are modeled by considering the delays caused by PMU measurement signals, the simulation of the studied system with two time delays of 350 and 500 milliseconds is shown in Figures 15 and 16. As shown, the fuzzy controller can dampen the fluctuations caused by SSR by considering the changes in fuzzy rules. In this simulation, we have k=75% & v=7m/s.

Table 6. Rule based on delay-compensated FLWADC

Time delay	Vc/V_c	PL	PM	PS	ZE	NS	NM	NL
M	P	PS	NL	PL	PM	PM	NM	PM
	N	NL	ZE	PM	NL	NS	NM	PS
	ZE	NS	PS	NM	ZE	PL	NM	NL
L	P	ZE	PM	PL	NM	NL	NM	PM
	N	PL	ZE	NM	PM	PM	PS	NM
	ZE	PS	NL	ZE	PL	NM	ZE	PL

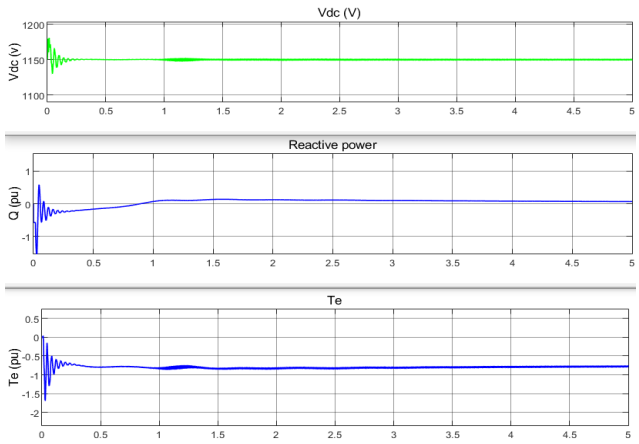

Fig. 14. Damping of capacitor voltage, reactive power and stator and electrical torque in k=75% & v=7m/s with new FLWADC and time delay equal to 350ms.

In the following, the performance of the proposed robust FLWADC is demonstrated. The system IEEE first benchmark model, modified by the inclusion of DFIG-based wind farms however, with time delays 350 ms and 500 ms in the feedback signals.

Fig. 13 shows capacitor voltage, reactive power and stator and electrical torque in k=75% & v=7m/s with new FLWADC and time delay equal to 350ms. When the FLWADC with time delay is in service, system is stable. Also, Fig. 14 shows capacitor voltage, reactive power and stator and electrical torque in k=75% & v=7m/s with new FLWADC and time delay equal to 500ms. These results demonstrate the effectiveness of the proposed auxiliary damping control (new FLWADC) in damping the SSR. Fig. 15 also shows that time delay assumed 500ms and effect of in latency ignored, hence system is unstable.

Fuzzy controller by using WAMS as an additional controller has been seen in few paper for damping SSR oscillations. so far, not been used WAMS by considering time delay (new FLWADC). The signals sent from PMU were studied and modeled, which in this paper is considered as a fuzzy input to the control system. For instance, in similar researches, measuring the control input parameters is considered virtually in the simulation, but the innovation of this research, in addition to using WAMS to measure the inputs of the fuzzy system, that brings closer to reality the controller.

6. CONCLUSION

In this study, a new method was used for damping SSR fluctuations of a DFIG- based wind farm with fuzzy controller and using WAMS by considering time delay (new FLWADC). Lack of adjusting the parameters of the controller, as well as working

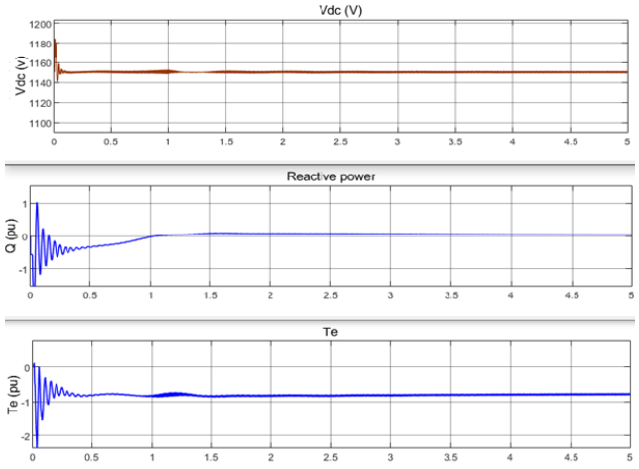

Fig. 15. Damping of capacitorvoltage, reactive power and stator and electrical torque in k=75% & v=7m/s with new FLWADC and time delay equal to 500ms.

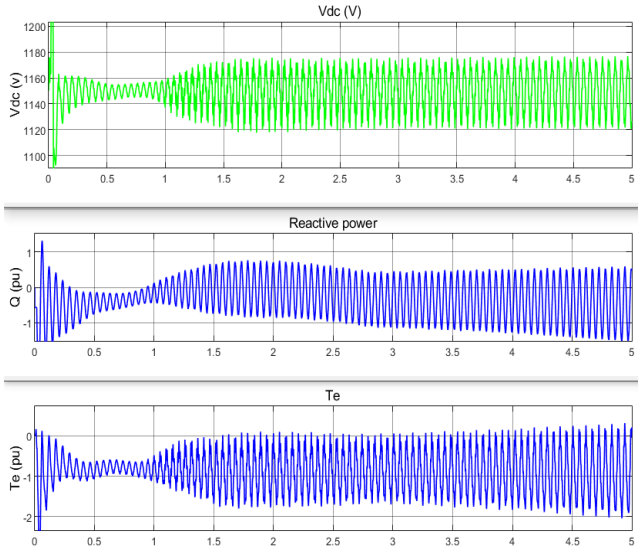

Fig. 16. capacitorvoltage, reactive power and stator and electrical torque in k=75% & v=7m/s with FLWADC ignored latency in time delay equal to 500ms .

at a high level of compensation, namely 75% and using WAMS by considering the delay caused by the PMU measurement is the main feature of this controller. Delay is important since it can cause system instability if ignored. The effect of this controller (new FLWADC) in damping SSR fluctuations was demonstrated by time simulation using Matlab/Simulink software on the modified version of the first benchmark model of the IEEE.

REFERENCES

1. [1] Lie X, Cartwright P. Direct active and reactive power control of DFIG for wind energy generation. IEEE Transactions on Energy Conversion 2006; 21 (3): 750-758. doi: 10.1109/TEC.2006.875472.
2. [2] R. Piwko, N. Miller, J. Sanchez-Gasca, X. Yuan, R. Dai, and J. Lyons, “Integrating large wind farms into weak power grids with long transmission lines,” in IEEE/PES Transmission and Distribution Conference & Exhibition: Asia and Pacific, Dalian, China, 2005.
3. L. Fan, C. Zhu, Z. Miao, and M. Hu, “Modal analysis of a DFIG-based wind farm interfaced with a series compensated network,” IEEE Trans. Energy Convers., vol. 26, no. 4, pp. 1010–1020, Dec. 2011.
4. [4] Lie X, Cartwright P. Direct active and reactive power control of DFIG for wind energy generation. IEEE Transactions on Energy Conversion 2006; 21 (3): 750-758. doi: 10.1109/TEC.2006.875472.
5. Mohammadpour HA, Santi E. Optimal adaptive sub-synchronous resonance damping controller for a series- compensated doubly-fed induction generator-based wind farm. IET Renewable Power Generation 2015; 9 (6): 669-681. doi: 10.1049/iet-rpg.2014.0155.
6. Sahni M, Badrzadeh B, Muthumuni D, Cheng Y, Yin H et al. Subsynchronous interaction in Wind Power Plants- part II: An ercot case study. In: IEEE Power and Energy Society General Meeting; San Diego, CA, USA; 2012. pp. 1-9.
7. Sahni M, Muthumuni D, Badrzadeh B, Gole A, Kulkarni A. Advanced screening techniques for Sub-Synchronous Interaction in wind farms. In: EEE PES Transmission and Distribution Conference and Exposition (T&D); Orlando, FL, USA; 2012. pp. 1-9.
8. Wang L, Xie X, Jiang Q, Pota HR. Mitigation of multimodal subsynchronous resonance via controlled injection of supersynchronous and subsynchronous currents. IEEE Transactions on Power Systems 2014; 29 (3): 1335-1344. doi: 10.1109/TPWRS.2013.2292597.
9. Xie H, Oliveira MMD. Mitigation of SSR in presence of wind power and series compensation by SVC. In: Power System Technology (POWERCON); Chengdu, China; 2014. pp. 2819-2826.
10. M. S. El-Moursi, B. Bak-Jensen, and M. H. Abdel-Rahman, “Novel STATCOM controller for mitigating SSR and damping power system oscillations in a series compensated wind park,” IEEE Trans. Power Electron., vol. 25, no. 2, pp. 429–441, Feb. 2010.
11. Liu H, Xie X, Li Y, Liu H, Hu Y. Mitigation of SSR by embedding subsynchronous notch filters into DFIG converter controllers. IET Generation, Transmission & Distribution 2017; 11 (11): 2888-2896. doi: 10.1049/iet-gtd.2017.0138.
12. L. Xu and Y. Wang, “Dynamic modeling and control of dfig-based wind turbines under unbalanced network conditions,” IEEE Trans. Power Syst., vol. 22, no. 1, pp. 314–323, Feb. 2007.
13. F. M. Hughes, O. Anaya-Lara, N. Jenkins, and G. Strbac, “A power system stabilizer for DFIG-based wind generation,” IEEE Trans. Power Syst., vol. 21, pp. 763–772, May 2006.
14. Suriyaarachchi DHR, Annakkage UD, Karawita C, Kell D, Mendis R et al. Application of an SVC to damp sub- synchronous interaction between wind farms and series compensated transmission lines. In: IEEE Power and Energy Society General Meeting; San Diego, CA, USA; 2012. pp. 1-6.
15. Boopathi VP, Muzamil AR, Kumudini DRP, Ramanujam R. Analysis and mitigation of subsynchronous oscillations in a radially-connected wind farm. In: Power and Energy Systems: Ttowards Sustanable Eenergy ; Bangalore, India.
16. Liu H, Xie X, Zhang C, Li Y, Liu H et al. Quantitative SSR analysis of series-compensated DFIG-based wind farms using aggregated RLC circuit model. IEEE Transactions on Power Systems 2017; 32 (1): 474-483. doi: 10.1109/TPWRS.2016.2558840.
17. Mohammadpour HA, Santi E. Sub-synchronous resonance analysis in DFIG-based wind farms: mitigation methods- TCSC, GCSC, and DFIG controllers-part II. In: IEEE Energy Conversion Congress and Exposition (ECCE); Pittsburgh, PA, USA; 2014. pp. 1550-1557.
18. Mohammadpour HA, Santi E. Modeling and control of gate-controlled series capacitor interfaced with a DFIG-based wind farm. IEEE Transactions on Industrial Electronics 2015; 62 (2): 1022-1033. doi: 10.1109/TIE.2014.2347007.
19. Mohammadpour HA, Shin YJ, Santi E. SSR analysis of a DFIG-based wind farm interfaced with a gate-controlled series capacitor. In: Twenty-Ninth Annual IEEE in Applied Power Electronics Conference and Exposition (APEC); Fort Worth, TX, USA; 2014. pp. 3110-3117.
20. B. Naduvathuparambil, M. C. Valenti, and A. Feliachi, “Communication delays in wide area measurement systems,” in Proc. 34th Southeastern Symp. Syst. Theory, Mar. 2002, pp. 118–122.
21. Shotorbani, A. M., Madadi, S., & Mohammadi-Ivatloo, B. (2018). Wide-area measurement, monitoring and control: Pmu-based distributed

wide-area damping control design based on heuristic optimization using digsilent power factory. In Advanced Smart Grid Functionalities Based on PowerFactory (pp. 211-240). Springer, Cham.
22. Mukherjee, Sayak, et al. "Scalable designs for reinforcement learning-based wide-area damping control." IEEE Transactions on Smart Grid 12.3 (2021): 2389-2401.
23. P. Korba, R. Segundo, A. Paice, B. Berggren, and R. Majumder, “Time Delay Compensation in Power System Control,” European Union Patent EP08 156 785, May 2008.
24. M. Mokhtari, F. Aminifar, D Nazarpour, S. Golshannavaz,” Wide-Area Power Oscillation Damping With a Fuzzy Controller Compensating the Continuous Communication Delays” , IEEE Transactions on Power Systems, Vol. 28, No. 2, may. 2013, pp. 1997-2005.
25. J. Momoh, X. Ma and K. Tomsovic, “Overview and Literature Survey of Fuzzy Set Theory in Power Systems,” IEEE Transactions on Power Systems, Vol. 10, No. 3, Aug. 1995, pp. 1676-1690.
26. K. Tomsovic, M. Tapper and T. Ingvarsson, "A Fuzzy Information Approach to Integrating Different Transformer Diagnostic Methods," IEEE Transactions on Power Delivery, Vol. 8, No. 3, July 2013, pp. 1638-1646.
27. Thirumalaivasan R. Janaki MR. Xu YJ. Kalman filter based detection and mitigation of subsynchronous resonance with SSSC. IEEE Transactions on Power Systems 2017; 32 (2): 1400-1409. doi: 10.1109/TPWRS.216572301.
28. Moharana A, Varma RK, Seethapathy R. SSR alleviation by STATCOM in induction-generator-based wind farm connected to series compensated line. IEEE Transactions on Sustainable Energy 2014; 5 (3): 947-957. doi: 10.1109/TSTE.2014.2311072.
29. Fan L, Miao Z. Mitigating SSR using DFIG-based wind generation. IEEE Transactions on Sustainable Energy 2012; 3 (3): 349-358. doi: 10.1109/TSTE.2012.2185962.
30. Mohammadpour HA, Ghaderi A, Mohammadpour H, Santi E. SSR damping in wind farms using observed-state feed- back control of DFIG converters. Electric Power Systems Research 2015; 123: 57-66. doi: 10.1016/j.epsr.2015.01.018.
31. Zhao B, Li H, Wang M, Chen Y, Liu S et al. An active power control strategy for a DFIG-based wind farm to depress the subsynchronous resonance of a power system. International Journal of Electrical Power & Energy Systems 2015; 69: 327-334. doi: 10.1016/j.ijepes.2015.01.002.
32. Mohammadpour HA, Santi E. SSR damping controller design and optimal placement in rotor-side and grid-side converters of series-compensated DFIG-based wind farm. IEEE Transactions on Sustainable Energy 2015; 6 (2): 388-399. doi: 10.1109/TSTE.2014.2380782.